Available online at www.sciencedirect.com
ScienceDirect
Journal of Sound and Vibration 308 (2007) 405–417
JOURNAL OF SOUND AND VIBRATION
www.elsevier.com/locate/jsvi

Modelling approaches for an ultrasonic percussion drill

C. Potthast*, J. Twiefel, J. Wallaschek

Heinz Nixdorf Institute, University of Paderborn, Fürstenallee 11, 33102 Paderborn, Germany

Accepted 28 March 2007
The peer review of this article was organised by the Guest Editor
Available online 18 May 2007

Abstract

This work deals with a novel piezoelectrically driven vibro-impact drilling tool which is designed to drill holes and take rock samples in NASA's future space missions. The drilling device consists of an ultrasonic transducer with a piezoelectric stack, a free flying mass and a drill stem. Excited by the high-frequency vibration of the transducer the free mass oscillates between the horn tip of the transducer and the drill stem. The shock waves in the drill stem caused by the impacts with the free mass affect hard and brittle materials so effectively that small holes can be performed with extremely low additional downforce and low power consumption. This paper provides measurements with a modified actuator which show an irregular motion of the free mass. For further optimization two model approaches are investigated: the finite element method and a discrete lumped parameter model. Each model is capable of predicting actuator's parts motion similar to measurements.

1. Introduction

A piezoelectrically driven vibro-impact drilling tool called ultrasonic/sonic driller/corer [1] has been developed by Jet Propulsion Laboratory, Pasadena. The device is designed to drill holes and take rock samples in NASA's future space missions [2]. In addition other applications are mentioned, for example applications in robotics [3] and utilizing for rock powdering [4]. The actuator is a simple three part design of a vibrating transducer, a free mass and a drill stem (see Fig. 1). The transducer is piezoelectrically driven and performs longitudinal vibrations in axial direction in the range of micrometres. For experimental investigations and modelling a vibration amplitude of 15 μm was chosen. In the centre of the horn is a small hole which is used for linear guidance of a drill stem. A disc-shaped free mass with a hole slides along the drill stem between the transducer tip and a shoulder on the drill stem. The function of the free mass can be described as a kind of frequency transformation, since the high-frequency vibration of the transducer is transformed to low-frequency impacts.

The tool has a couple of advantages which make it interesting especially for space missions. The tool design is very simple and contains only a few moving parts. The weight is very low which is an extremely important

*Corresponding author. Tel.: +49 5251 606275; fax: +49 5251 606278.
E-mail address: potthast@hni.upb.de (C. Potthast).

0022-460X/$ - see front matter © 2007 Elsevier Ltd. All rights reserved.
doi:10.1016/j.jsv.2007.03.045

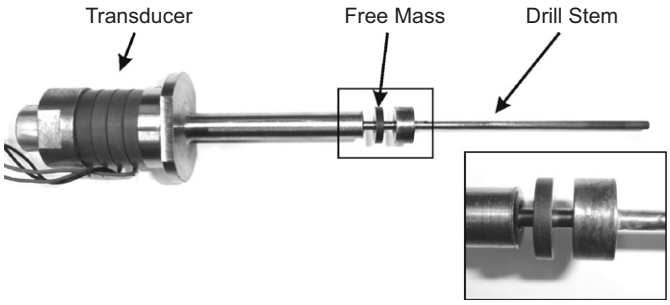

Fig. 1. Ultrasonic/sonic driller/corer with disc-shaped free mass.

aspect in consideration of transportation into outer space. The drill stem needs no cutting edge and therefore no tool wear occurs. Another fact which punctuates the low maintenance is that no lubrication is necessary. The actuator operates without rotation, hence bore holes with arbitrary cross sections are possible. The low power consumption is the tool's most important advantage. It has been demonstrated that a bore hole can be carried out with a minimum power consumption of only 5 W [2].

So far the drilling device has demonstrated its functional efficiency, but the complex nonlinear dynamics of the actuator and the mechanism which is responsible for the drilling progress are not understood satisfactorily. A systematic design of a tool with optimized drilling performance is therefore unfeasible until now.

The motivation for this work is to investigate if the actuator can be an appropriate drilling tool for terrestrial applications. For this reason the actuator is analysed by means of models and investigated experimentally. Besides recent experimental results the paper describes two model approaches and the associated results.

2. Measurements

The construction with a disc-shaped free mass as described in the introduction has been investigated experimentally in Ref. [5]. The impacts between free mass and transducer as well as between free mass and drill stem has been logged over time by employment of an electrical contact detection circuit. A video of the working actuator revealed that the free mass performs a significant wobbling action which makes the detailed interpretation of the measured contact signal futile. Nevertheless some important conclusions could be drawn which are also observed in the measurements presented in this section.

Since the wobbling action of the free mass is an unwanted effect the disc-shaped free mass was replaced by a steel ball. In order to guide the ball along the axial direction the top of the drill stem is formed as a cylinder. Fig. 2 shows the modified actuator. For motion observation of the free mass the tube has two elongated holes.

The transducer is clamped at the nodal point in the test rig shown in Fig. 3. The test rig is used to guide the transducer as well as to apply downforces. The additional forces are applied by means of a weak spring connected with a wire which is turned round in order to pull the transducer downwards. Transducer and drill stem are made of steel, the ball is 8 mm in diameter and is taken from a ball bearing. The transducer is driven in resonance with a phase locked loop controller [6] realized with common laboratory equipment. The resonance frequency is about 20.1 kHz. The vibration amplitude was about 15 μm.

High-speed camera videos are used to pursuit the movement of transducer tip, free mass and drill stem by point tracking. Fig. 4 contains diagrams for different downforces applied on the transducer. Diagrams (a), (b), (c) and (d) correspond to 0, 3, 6 and 9 N additional force. 0 N means that only self-weight (≈ 300 g) due to gravity is present. The dotted line depicts the movement of the transducer tip, the solid line represents the free mass movement and the dashed line shows the motion of the impact surface of the drill stem. The measured displacements do not contain the outer dimensions of the three bodies because they were eliminated from the data before plotting. Therefore, all curves will show zero displacement when the three parts rest upon each other.

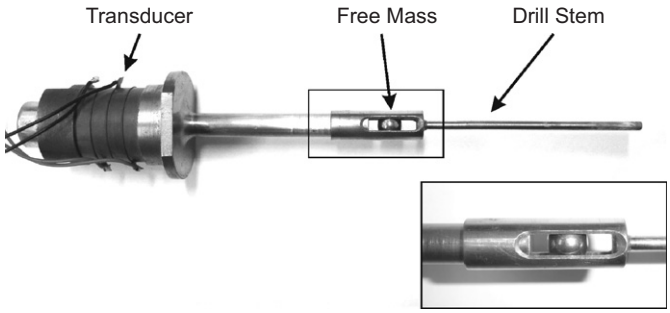

Fig. 2. Modified Ultrasonic/sonic driller/corer.

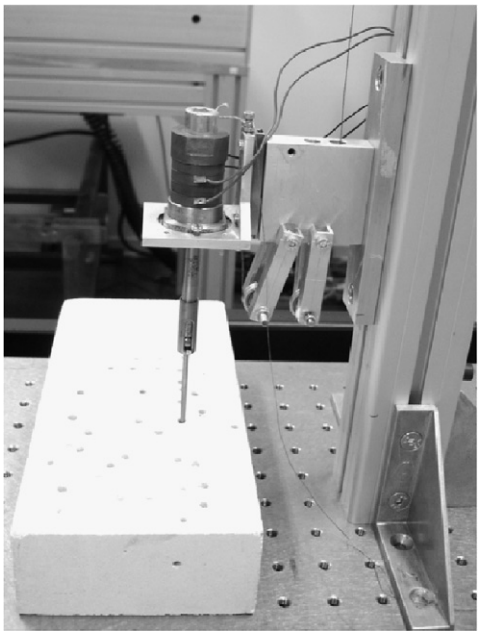

Fig. 3. Ultrasonic driller in test rig.

Since the resolution of the camera is limited (128×256 pixel at a frame rate of 9000 frames per second) and moreover distinct rigid body movements in the millimetre range are superimposed the ultrasonic vibration of the transducer tip is not visible though still present. First, the measurements reveal a distinct irregular motion. It should be pointed out that this is a permanent irregularity and not due to a transient response before reaching a steady state. As can be seen in the figures the transducer is catapulted a couple of millimetres upwards and falls down again due to gravity and applied force. Because the drill stem is not pressed upon the surface separately noteworthy motion of the drill stem is also present. With higher downforces the rigid body motion of the transducer decreases while the frequency of the free flight periods raises. Besides the free mass demonstrates more action when higher downforces are present. The typical parabolic free flight motion of the transducer is sometimes changed due to impacts with the free mass.

The measurements were accomplished while the actuator was operating upon a force sensor. The measured force signals are shown in Fig. 5 for the same four downforces mentioned above. Though the measured contact force value is not directly related to material removal in the drilled rock it gives a good impression of the mechanism responsible for drilling progress. If only self-weight is active the impact of the falling transducer is the main mechanism. At highest downforce the free mass's impacts with the drill stem will also have a contribution to material removal.

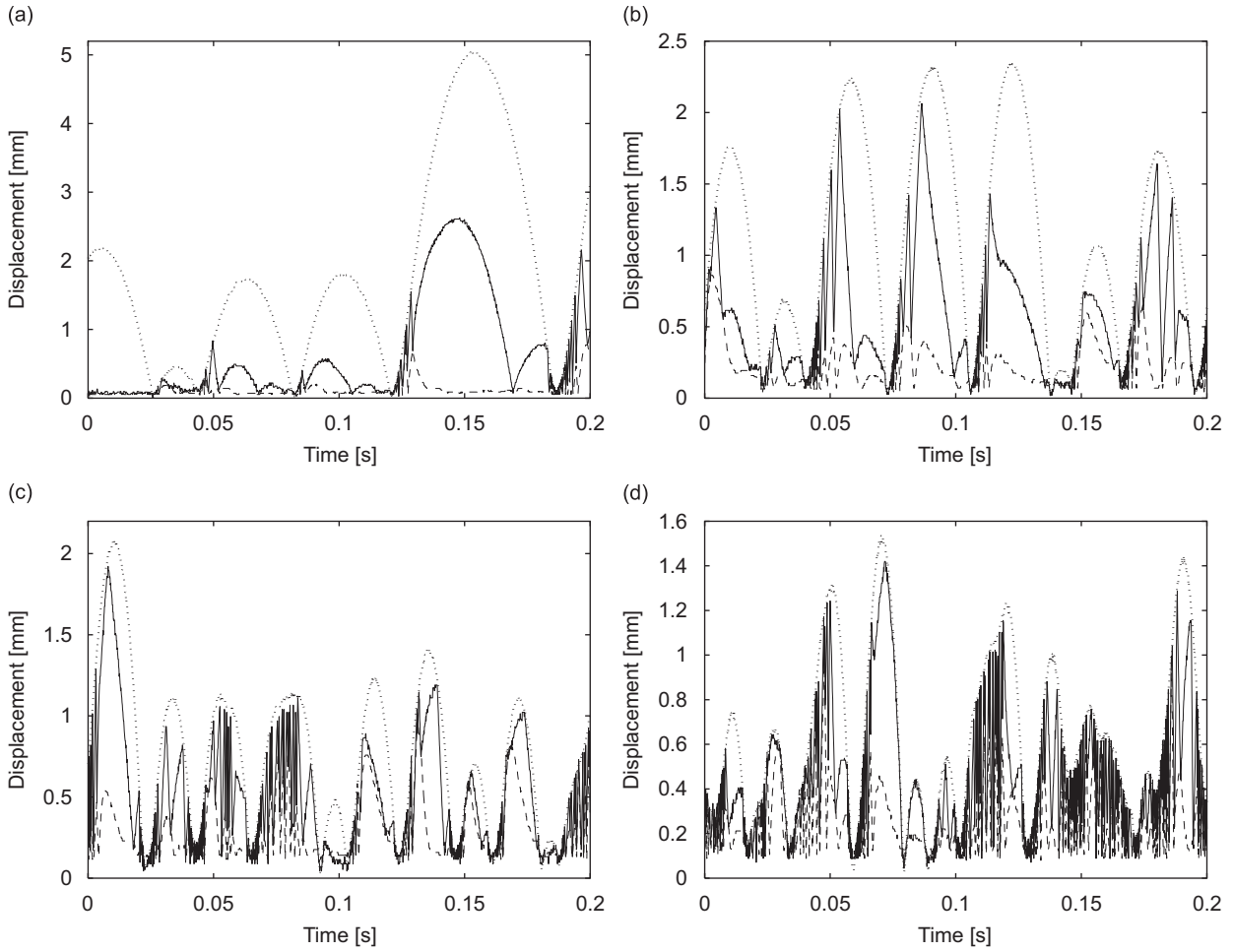

Fig. 4. Displacement of transducer tip, free mass and drill stem: (a) only self-weight, (b) 3 N downforce, (c) 6 N downforce, (d) 9 N downforce. ····· transducer tip, ——— free mass, – – – – drill stem.

3. Modelling

Currently, the effects of parameters like weight of the free mass, vibration amplitude of the transducer tip, vibration frequency or transducer weight are unknown. Because optimizing the actuator for terrestrial applications is the primary goal there is the need for developing models which allow parameter variations easily. Many different classes of models for dealing with impact problems are known. A good overview can be found in Ref. [7]. Since the drilling actuator is a complex device with three contact areas, the initial model must simply be capable of describing the global dynamics of the actuator detailed in the previous section. For comparison with measurements it must be possible to simulate at least a few hundred milliseconds. Two modelling approaches will be described in the following: a finite element model and a discrete lumped parameter model with visco-elastic Kelvin–Voigt elements.

3.1. Finite element model

The finite element method is widely used for the design of piezoelectric actuators. Many commercial finite element codes allow simulation of electrical–mechanical coupling necessary for emulation of piezoelectric material behaviour. For actuator design mainly linear modal analyses are used to determine eigenfrequencies

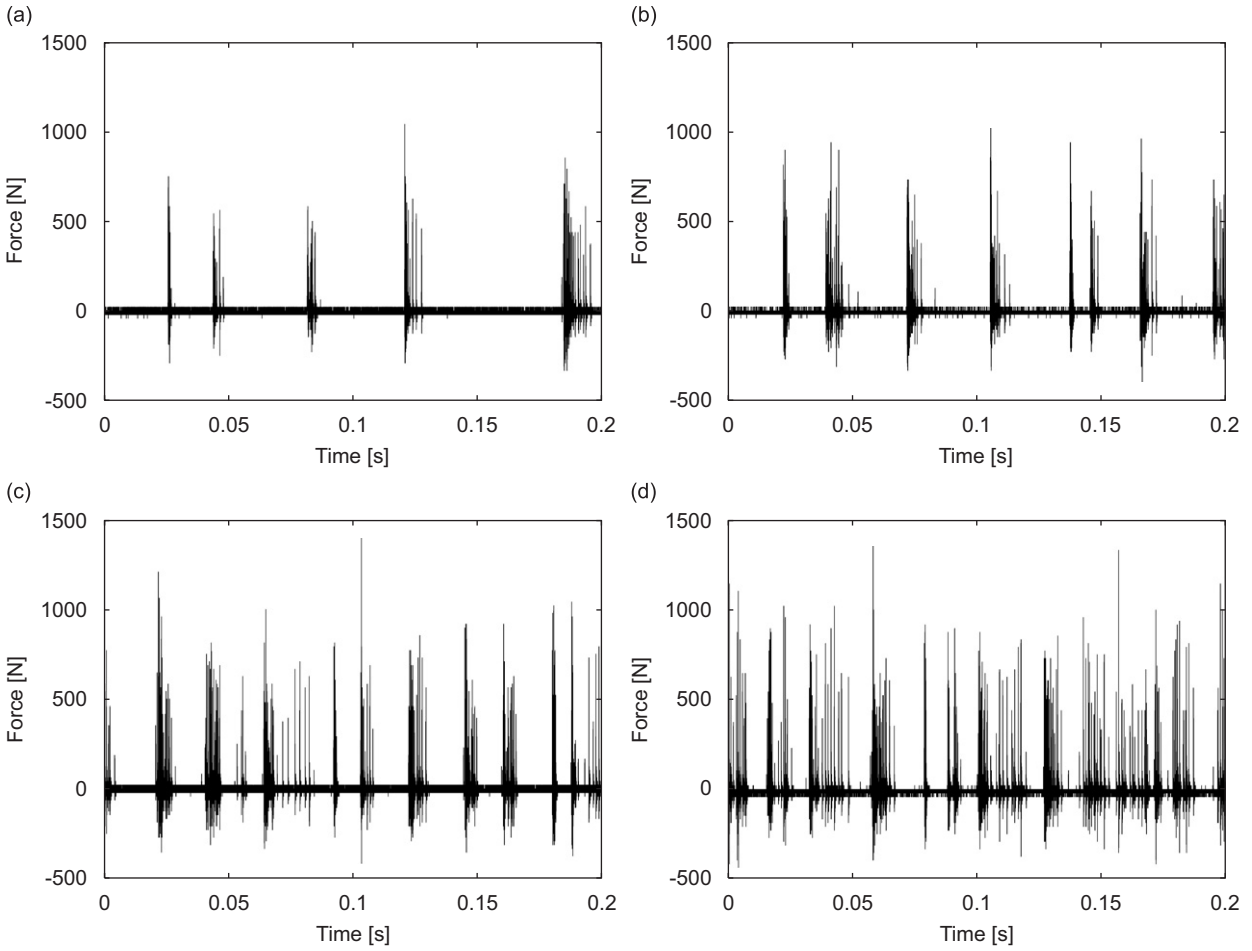

Fig. 5. Contact force between drill stem and surface: (a) only self-weight, (b) 3 N downforce, (c) 6 N downforce, (d) 9 N downforce.

and modes of vibration. In general the finite element method is an excellent technique for analysis of a specific actuator design. Since the modelling effort is usually very high the typical procedure is to use simple models for a coarse dimensioning and afterwards the finite element method for verification or further detailing.

Most applications of piezoelectric actuators are based upon contact processes, for example ultrasonic motors. Contact modelling is always the bottleneck because no standard modelling technique has been established. The benefit of finite element modelling has been proven especially in transducer design [8] but using finite elements for simulation of a complete actuator including contact remains the exception. When finite elements are used for impact problems typically simple setups like impact of spheres against rods [9] or half-spaces [10] are investigated. The approach in this work is to investigate if the finite element method is able to reproduce the global dynamics of the considered actuator. The transient calculation method is examined primarily in view of basic applicability. For the calculations presented here the ANSYS 10.0 implicit finite element program was used. Most commercial explicit codes like ABAQUS/Explicit or LS-DYNA are not capable of piezoelectric field coupling simulation. Though piezoelectric actuators are not the principle application of explicit codes, a few works demonstrate the applicability, e.g. Ref. [11]. Due to the absence of piezoelectric elements the vibration excitation has been realized via thermal excitation, which is an alternative method of using field coupling in the finite element method. Compared to the more obvious possibility of vibration excitation via a sinusoidal external force, thermal excitation has the advantage that the direction of the resulting strains needs not to be known beforehand.

3.1.1. Full transient method

Extensive treatment of the theory of the finite element method will not be presented here since many excellent sources of data regarding this technique may be found in literature. To solve the equation of a dynamic FE system

$$\mathbf{M}\ddot{\mathbf{u}}_n + \mathbf{C}\dot{\mathbf{u}}_n + \mathbf{K}\mathbf{u}_n = \mathbf{F}_n^a \tag{1}$$

implicit algorithms use an iterative time-stepping method to compute the displacement:

$$\mathbf{u}_{n+1} = f(\dot{\mathbf{u}}_{n+1}, \ddot{\mathbf{u}}_{n+1}, \mathbf{u}_n, \dot{\mathbf{u}}_n, \ddot{\mathbf{u}}_n, \ldots), \tag{2}$$

where $\mathbf{M}$ represents the global mass matrix, $\mathbf{C}$ is the global damping matrix, $\mathbf{K}$ is the global stiffness matrix, the vector $\mathbf{u}_n$ and its derivatives with respect to time $\dot{\mathbf{u}}_n$ and $\ddot{\mathbf{u}}_n$ represent nodal displacement, velocity and acceleration at time t_n. $\mathbf{F}_n^a$ is the vector of applied external loading at time t_n. The so-called full transient method uses the full system matrices in order to calculate the system response. The full method is the most powerful method since all kinds of nonlinearity can be included: nonlinearities in boundary conditions (contact), nonlinearities in material (plasticity, nonlinear viscosity) and geometric nonlinearities (large displacements). The actual model includes nonlinearities in boundary conditions and geometry. The material behaviour is modelled as pure elastic.

Fig. 6 shows a cut-out of the used finite element mesh. A 2D-axisymmetric model is used since unsymmetries of the actuator are negligible. The surfaces of ball, transducer tip and top of the drill stem are covered with contact element layers. A third contact is modelled between the bottom of the drill stem and the surface. The solid elements are high-order elements with 8 nodes as these elements cause less convergence problems than the low-order elements with 4 nodes. However, computation time increases because calculation effort in implicit algorithms is approximately proportional to n^2, where n is the number of degrees of freedom in the model. The total number of nodes used is 1844, the total number of elements is 504. Apart from the contact areas the mesh is rather coarse in order to save computation time. Since wave propagation or stresses at specific locations are not in the focus of this work directives for proper spatial discretization mentioned for example in Ref. [12] are not followed strictly for the advantage of faster computation. As contact algorithm the penalty method is used, where springs are added between overlapping nodes to generate the contact force. For realistic results it is necessary that in each contact phase a couple of nodes come into contact. This is achieved by a slight flattening of the ball at contact zones and by a mesh refinement in the areas of interest, see Fig. 6. The piezoelectric stack of the transducer is voltage excited. Damping is applied as material damping β_j for each material separately and as an additional stiffness proportional parameter β of global rayleigh damping. The damping matrix $\mathbf{C}$ has the following form:

$$\mathbf{C} = \alpha\mathbf{M} + \beta\mathbf{K} + \sum_{j=1}^{N_{\mathrm{MAT}}} \beta_j \mathbf{K}_\mathbf{j}, \tag{3}$$

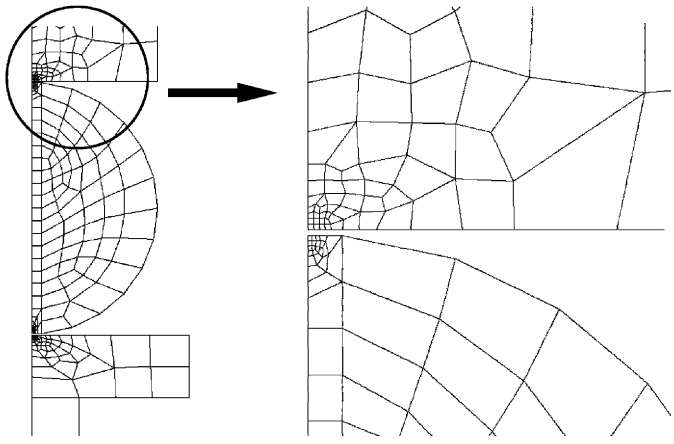

Fig. 6. Finite element mesh used in the full transient analysis.

where α is the mass proportional rayleigh damping parameter representing damping of the rigid body motion ($\alpha = 0$ was used in this application), N_{MAT} is the number of different materials and $\mathbf{K}_j$ is the portion of structure stiffness matrix based on material j. Numerical values for the material damping parameter β_j are calculated by

$$\beta_j = \frac{1}{\omega Q_{m_j}}, \tag{4}$$

where $\omega = 2\pi f$ is the eigen angular frequency in Hz and Q_{m_j} is the mechanical quality factor of the specific material j taken from literature ($Q_m = 1000$ for steel, $Q_m = 400$ for piezo). The rayleigh damping parameter $\beta = 8 \times 10^{-9}$ s was adapted to achieve good agreement to measurements.

Dependant on the applied damping the transient behaviour before the transducer reaches its steady state can take several milliseconds. In order to reduce computation time a method was developed that allows the transient calculation starting in the steady state. To achieve this first a modal analysis is carried out. The calculated eigenfrequency is used afterwards in a harmonic analysis which computes the vibration amplitude in the steady state for excitation with a voltage of 1 V at the given eigenfrequency. The amplitude is used to calculate a scaling factor for excitation voltage which will make the transducer vibrate with the desired amplitude. Besides the displacement results of the harmonic analysis are applied to the model as initial conditions. Compared to the multitude of transient load steps necessary for reaching the steady state the effort for a single modal analysis and a single harmonic analysis is negligible.

Numerical convergence problems often arise during change in contact state. Primarily in the change from non-contact to contact. During these time periods small time steps are required. For a free sinusoidal vibration without contact 20 time steps per cycle are sufficient. During closed contact at least 20 time steps should be computed. An automatic time stepping algorithm has been implemented which distinguishes each load step between open or closed contact and if the contact status will change during the next time period or not. For the considered model this results in a time step of 2.5×10^{-6} s for non-contact, 8.3×10^{-7} s for contact and 2.5×10^{-8} s for the period in which contact status changes.

Despite the efforts in time step adaption convergence problems could not be avoided completely. Calculation results are shown in Fig. 7. In the beginning the contacts are open. All three parts start with a distance of 50 μm and fall down due to gravity. The extensive overlapping in displacements especially between 5 and 8 ms results from contact stiffness being too low. However, after roughly 31 000 load steps and approximately 20 ms simulated time the calculation terminated because of convergence problems. Computation time on a usual personal computer (AMD X2 4200+, 2.2 GHz) was approximately 7 h (1300 s per simulated millisecond). Though the contact stiffness was too low, the result looks reasonable. Primarily

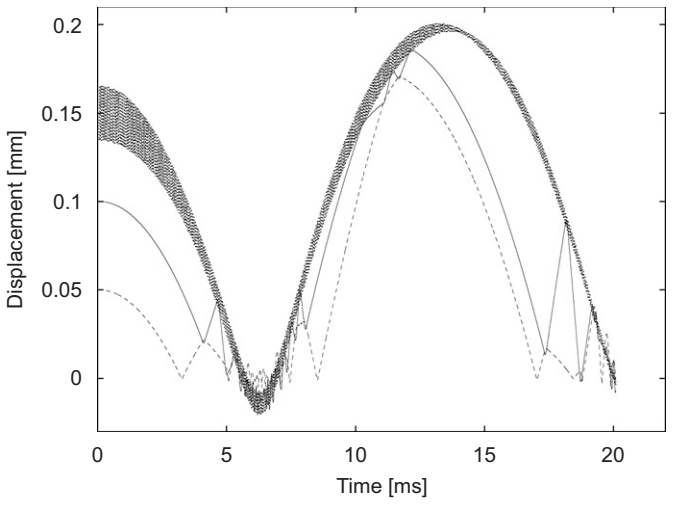

Fig. 7. Displacement results for full transient calculation. ····· transducer tip, —— free mass, –––– drill stem.

due to the extreme computation time and secondarily due to convergence problems it has been judged as senseless to make further efforts in parameter adaption or elongation of simulated time.

3.1.2. Reduced transient method

The ANSYS program offers the possibility of carrying out a so-called reduced transient analysis which allows condensation of the model size by application of master degrees of freedom and reduced matrices. After displacements of the master degrees of freedom have been calculated the solution can be expanded to all original degrees of freedom. The reduced method is applicable for linear transient calculations. The only applicable nonlinearity is the simple contact between nodes by means of gap elements. The main advantage of the reduced method is the fast computation. Main disadvantages are the restriction in nonlinearities mentioned above and the impossibility to apply element loads which makes emulation of piezoelectric behaviour unaccessible. Gap elements act as springs if distance between adjacent nodes falls below a defined gap size. Each of the three contacts in the actuator is provided with a gap element with a specific stiffness. Damping cannot be applied via gap elements in a reduced analysis. Therefore a global rayleigh damping formulation is used. Convergence problems do not arise in the reduced transient method. A similar model is used as in the full method except for the fact that the mesh is not refined near contact areas, see Fig. 8.

Low-order elements with 4 nodes are used. The whole model consists of 237 nodes and 135 elements. Since piezoelectrically excited ceramics cannot be simulated a force excitation is chosen. The force is adapted to result in the same vibration amplitude as the voltage excitement does.

Results for different downforces are given in Fig. 9. An irregular motion similar to the measurements is observed. The maximum flying heights of the transducer are in good agreement to measurements. It must be taken into account that for reasons of clarity only 200 ms are shown in all diagrams. Higher maximum displacements may occur in calculations and measurements as well. However, the fundamental behaviour remains the same. The drastic reduction of computation time—approximately 6 s per simulated millisecond—makes adapted time steps dispensable.

3.2. Discrete model

The models described in the previous section allow parameter variations only in a limited manner. Therefore an additional discrete lumped parameter model approach is chosen. The transducer operates at resonance in a

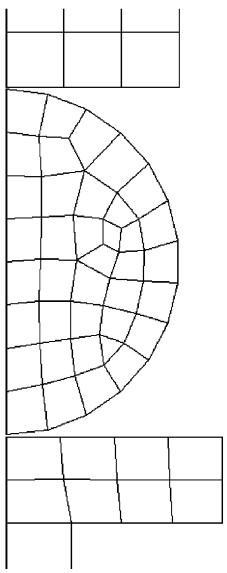

Fig. 8. Finite element mesh used in the reduced transient analysis.

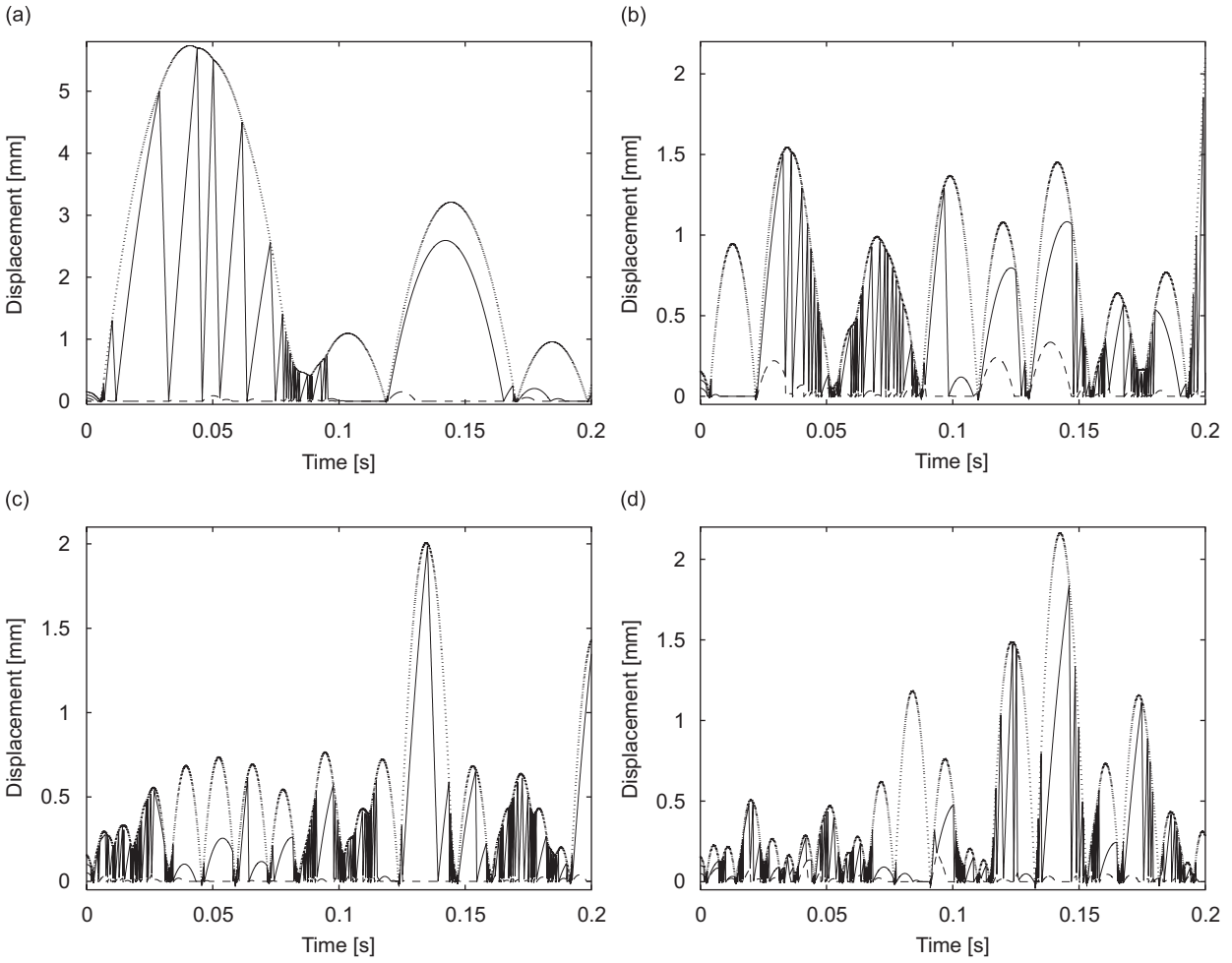

Fig. 9. Displacement results for reduced transient calculation: (a) only self-weight, (b) 3 N downforce, (c) 6 N downforce, (d) 9 N downforce. ····· transducer tip, —— free mass, – – – – drill stem.

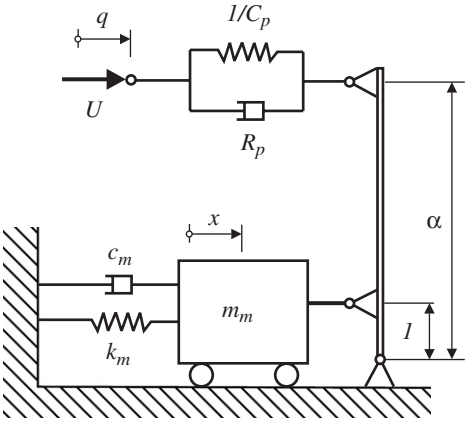

Fig. 10. 1-dof equivalent mechanical model of a piezoelectric actuator near resonance.

dominant longitudinal vibration mode. For this mode the system can be described with the 1-dof equivalent mechanical model of a piezoelectric actuator near resonance [13] shown in Fig. 10.

In the equivalent model the mass m_m represents the modal mass of the transducer at its resonance frequency, the spring k_m represents the modal stiffness and c_m is the modal damping. The spring $1/C_p$ is the equivalent of the electrical capacitance of the piezoelectric transducer. The damper R_p takes dielectric losses into account. In most practical cases the dielectric losses can be neglected. The parameters can be identified by measuring the electrical and the mechanical admittances I/U and v/U, where I and U are current and voltage and $v = \dot{x}$ is the velocity of the transducer tip. A detailed description of the identification process can be found in Ref. [14]. This actuator model has the disadvantage that it represents a free vibrating transducer without rigid body movement. The measurements in Section 2 demonstrate clearly that modelling of the rigid body motion is of decisive importance.

In Fig. 11 the piezoelectric actuator model (System *I*) is extended with a single mass m_t (System *II*). This mass reflects the self-weight of the transducer. The vibration (coordinate x) is superimposed onto the rigid body motion (coordinate z). Below the transducer model are single masses representing free mass (System *III*) and drill stem (System *IV*). Each with a spring and a damper in parallel (Kelvin–Voigt model). The surface is modelled by a spring–damper system fixed to the environment (System *V*). Gravitational forces are applied to each system except for System *I*. The equations of motion for systems *I–IV* are as follows:

$$m_m\ddot{x} + c_m\dot{x} + k_m x = F_{c1} - F_a - \alpha U, \tag{5}$$

$$m_t\ddot{z} = F_{c1} - F_a - m_t g, \tag{6}$$

$$m_f\ddot{w} = -F_{c1} + F_{c2} - m_f g, \tag{7}$$

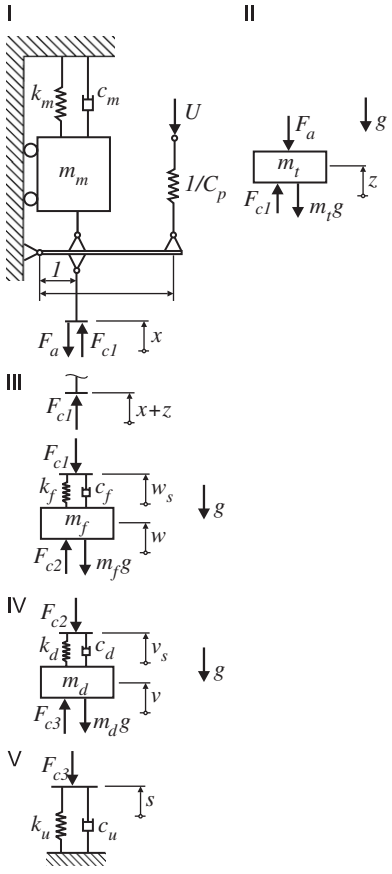

Fig. 11. Mechanical model of the drill with spring–damper systems as contact layers.

$$m_d\ddot{v} = -F_{c2} + F_{c3} - m_d g. \tag{8}$$

For closed contact the resulting contact forces are calculated by

$$F_{c1} = c_f \Delta\dot{w} + k_f \Delta w, \tag{9}$$

$$F_{c2} = c_d \Delta\dot{v} + k_d \Delta v, \tag{10}$$

$$F_{c3} = c_u \dot{v} + k_u v, \tag{11}$$

where Δw and Δv denote

$$\Delta w = w - w_s \quad \text{and} \quad \Delta v = v - v_s. \tag{12}$$

Besides the following coordinates are set when contact is closed:

$$w_s \equiv x + z, \tag{13}$$

$$v_s \equiv w, \tag{14}$$

$$s \equiv v. \tag{15}$$

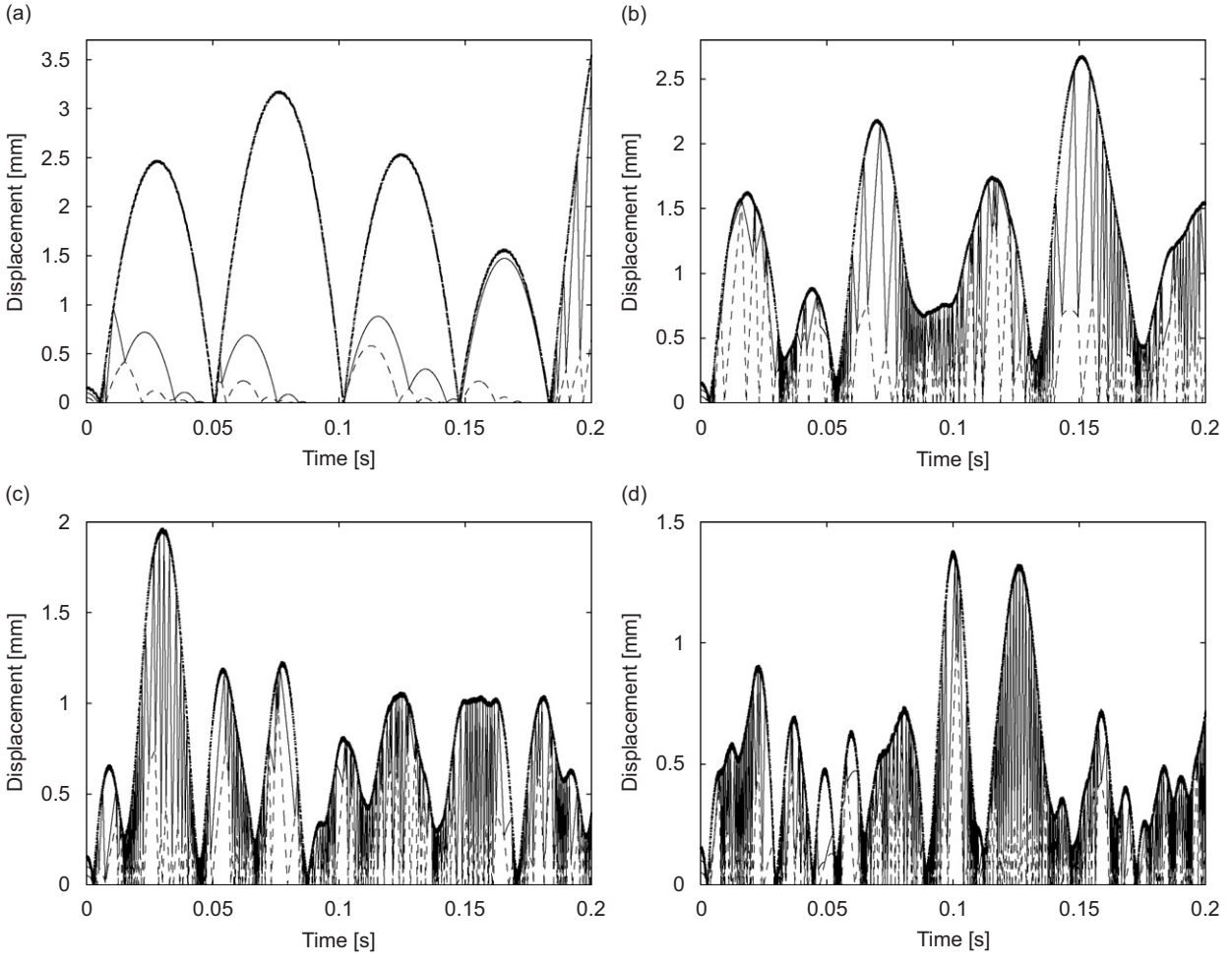

Fig. 12. Displacement results for discrete model: (a) only self-weight, (b) 3 N downforce, (c) 6 N downforce, (d) 9 N downforce. ····· transducer tip (coordinate $x + s$), ——— free mass (coordinate w_s), – – – – drill stem (coordinate v_s).

For open contact the corresponding forces are set to zero: $F_{c1} \equiv 0$ and/or $F_{c2} \equiv 0$ and/or $F_{c3} \equiv 0$. The equation for the surface coordinate s is

$$c_u\dot{s} + k_u s = 0. \tag{16}$$

The transition from open to closed contact is determined by the coordinates $x + z$ and w_s, w and v_s as well as v and s. The transition from closed to open contact is identified by a negative or zero contact force. The model is implemented in Matlab/Simulink. A variable time step size is chosen which is set to be between 4.8×10^{-7} s and 9.5×10^{-9} s.

Fig. 12 shows the computed displacements of the discrete model. It turns out that result in similarly good quality can be achieved as in the reduced finite element method. Due to the three spring-damper systems the possibility for parameter adaption to measurements is better than in the reduced finite element method. Less computation time (2.6 s per simulated millisecond) is another advantage of the discrete model.

4. Conclusions

Two model approaches have been investigated. The full transient finite element method is difficult to handle because working solution parameters must be found. The convergence problem and the extremely long computation time make this method even more troublesome to use. Reduced finite elements with gap elements and the discrete model are promising model approaches with bearable expense in modelling and computation time. The discrete modelling approach also gives good results. In order to quantify the accuracy of model predictions currently steps are underway to apply statistical methods. Next steps will aim at more accurate parameter identification in simplified experiments and model verification. A subsequent study of the influence of different actuator parameters, e.g. vibration amplitude, vibration frequency and weight of the free mass, will give insights into the optimization potential of drilling device.

Though the discrete model comes with less effort in modelling and shorter computation time the finite element method still has its benefits, e.g. inclusion of wave propagation without additional modelling effort. Concerning the finite element method explicit solution techniques may be worth to be taken into account because of their fastness and numerical robustness. A mixed approach with rigid bodies and a modal Galerkin formulation for the transducer has already been begun.

References

[1] Y. Bar-Cohen, S. Sherrit, B.P. Dolgin, D. Pal, J. Kroh, T. Peterson, Smart-ultrasonic/sonic driller/corer, World Patent No. WO 01/83933 A1, November 2001.

[2] Y. Bar-Cohen, S. Sherrit, B.P. Dolgin, D. Pal, J. Kroh, T. Peterson, Ultrasonic/sonic driller/corer (USDC) as a sampler for planetary exploration, *Proceedings of the IEEE Aerospace Conference on the topic of Missions, Systems, and Instruments for In Situ Sensing*, 2001.

[3] M. Badescu, X. Bao, Y. Bar-Cohen, Z. Chang, B.E. Dabiri, B. Kennedy, S. Sherrit, Adapting the ultrasonic/sonic driller/corer (USDC) for walking/climbing robotic applications, *Proceedings of the SPIE Smart Structures Conference*, Vol. 5764-37, SPIE, 2005.

[4] S.J. Chipera, D.T. Vaniman, D.L. Bish, P. Sarrazin, S. Feldman, D.F. Blake, G. Bearman, Y. Bar-Cohen, Evalution of rock powdering methods to obtain fine-grained samples for chemin, a combined XRD/XRF instrument, *Lunar and Planetary Science Conference*, Houston, 2004.

[5] C. Potthast, Charactisation and system analysis of a novel ultrasonic percussion drill, *Proceedings of the 2nd International Workshop on Piezoelectric Materials and Applications in Actuators*, Paderborn, Germany, 2005, pp. 155–161.

[6] W. Littmann, T. Hemsel, C. Kauczor, J. Wallaschek, M. Sinha, Load-adaptive phase-controller for resonant driven piezoelectric devices, *World Congress Ultrasonics*, Paris, 2003.

[7] W.J. Stronge, *Impact Mechanics*, Cambridge University Press, Cambridge, 2000.

[8] N.N. Abboud, G.L. Wojcik, D.K. Vaughan, J. Mould, D.J. Powell, L. Nikodym, Finite element modeling for ultrasonic transducers, *Proceedings of the SPIE International Symposium on Medical Imaging*, San Diego, 1998.

[9] R. Seifried, W. Schiehlen, P. Eberhard, Numerical and experimental evaluation of the coefficient of restitution for repeated impacts, *International Journal of Impact Engineering* 32 (2005) 508–524.

[10] C. Wu, L. Li, C. Thornton, Rebound behaviour of spheres for plastic impacts, *International Journal of Impact Engineering* 28 (2003) 929–946.

[11] A. Frangi, A. Corigliano, M. Binci, P. Faure, Finite element modelling of a rotating piezoelectric ultrasonic motor, *Ultrasonics* 43 (2005) 747–755.

[12] R. Seifried, B. Hu, P. Eberhard, Numerical and experimental investigation of radial impacts on a half-circular plate, *Multibody System Dynamics* 9 (2003) 265–281.
[13] J. Krome, J. Wallaschek, Reduktion kontinuumsmechanischer Modelle im Rahmen der Optimierung mechatronischer Systeme am Beispiel des Wanderwellenmotors. VDI-Bericht 1315 ''Mechatronik im Maschinen und Fahrzeugbau,'' 1997, pp. 75–90.
[14] W. Littmann, Piezoelektrische, resonant betriebene Ultraschall-Leistungswandler mit nichtlinearen mechanischen Randbedingungen. PhD Thesis, Heinz Nixdorf Institute, University of Paderborn, 2003.